

HT2008-56259

NUMERICAL PREDICTION OF THE TEMPERATURE DISTRIBUTION WITHIN A HUMAN EYE DURING LASER SURGERY

Sandeep Singh Kushwaha and P.S.Ghoshdastidar
Department of Mechanical Engineering
Indian Institute of Technology Kanpur
Kanpur, U.P.208016
INDIA
E-Mail: psg@iitk.ac.in

ABSTRACT

In this paper a computational heat transfer model for prediction of the temperature distribution within the human eye during laser surgery is presented. The heat transfer within a tissue is described by the classic Pennes bioheat transfer equation. The intraocular temperature distribution is calculated using finite-difference method. Two types of computational domain have been considered: (i) rectangular parallelepiped and (ii) cylindrical. The eye is modeled as a composite layered structure consisting of four different ocular tissues, namely, cornea, aqueous, lens and vitreous. It is assumed that the eye is symmetrical about the pupillary axis. The absorption probability of ocular tissue is modulated based on the Lambert-Beer's law to reproduce the exponential attenuation of the laser light with depth within a biomaterial. The heat flow is modeled as transient and three-dimensional for rectangular parallelepiped geometry and two-dimensional (axi-symmetric) for the cylindrical geometry. The results indicate that for the insulation condition imposed on the periphery of the eye the model based on rectangular parallelepiped geometry of the eye at no laser power and at the initial temperature of 25°C predicts temperature closer to in-vitro experimental measurements reported in literature whereas the model based on cylindrical geometry predicts higher temperature. The opposite is true (that is, lower temperature is predicted by the model based on cylindrical geometry) for high laser heat flux (2000 W/m²) and higher initial temperature (37°C). This study also presents changes in eye temperature subjected to intermittent laser source used in laser surgery techniques such as PRK and LASIK. A comparison of the results based on three different boundary conditions such as convection ($h_b = 10 \text{ W/m}^2\text{K}$), constant temperature (37°C) and insulation on the eye periphery reveals that the model based on insulation condition predicts results closer to that of in-vitro experiment at no laser power and initial temperature of 25°C whereas at a laser power of 200 W/m² and at the initial temperature of 37°C insulation boundary condition produces highest temperature followed by that produced by convection and constant temperature conditions. The heat transfer is one-dimensional for the insulated eye periphery whereas multi-dimensional heat flow takes place when the circumferential boundary condition is either convective or isothermal.

1.0 INTRODUCTION

The word "laser" is an acronym for Light Amplification by Stimulated Emission of Radiation. Lasers are playing increasingly important role in medical applications such as surgery. One such application is the reshaping of the cornea. People with conditions such as short and long sightedness have benefited from laser eye surgery. The restoration of normal

vision is the aim of laser eye surgery. In the procedure called Photorefractive Keratectomy (PRK) the outer layer of the cornea, also called epithelium, is removed and an excimer laser is used to reshape underneath tissue. In a newer procedure called Laser-assisted in-situ Keratomileusis (LASIK) a microkeratome is used to cut a flap in the corneal tissue. In the end the flap is put back to its place. The excimer laser is a special type of laser that does not burn the corneal

tissue, but vaporizes a small quantity of the cornea each time a beam is pulsed onto the eye surface. The laser beam used in this type of surgery has wavelengths in the infrared range which is 700 nm to 1 mm as in this range the action is primarily thermal.

Eye is the most important part of human body and temperature has a profound effect on the eye. A sectional view of the eye [26] is shown in Fig.1. During eye surgery by laser source, temperature of eye changes because of absorption of high intensity irradiation of light. This elevated temperature can cause injury to the eye [24, 7, 5]. The tissues most vulnerable in the eye are the cornea and aqueous humor as the infrared radiation raises the overall temperature of the aqueous eye [19]. Therefore, the prediction of temperature profile even before eye surgery is carried out can be useful to doctors and it would minimize intraocular tissue thermal damage. Since measurement of temperature of the live human eye during laser surgery is very difficult computer models can be developed to study the heat flow inside human eye during the surgical operation.. A model typically has the following features. (a) Each tissue or fluid compartment of the eye is designated by its appropriate thermophysical properties; (b) Realistic boundary and tissue interface conditions are imposed; (c) Realistic environmental conditions are included; (d) Eye is modeled as far as possible close to the realistic shape; (e) The energy absorption within ocular tissues is modeled based on the Lambert-Beer's law to reproduce the exponential attenuation of the laser light within a biomaterial.

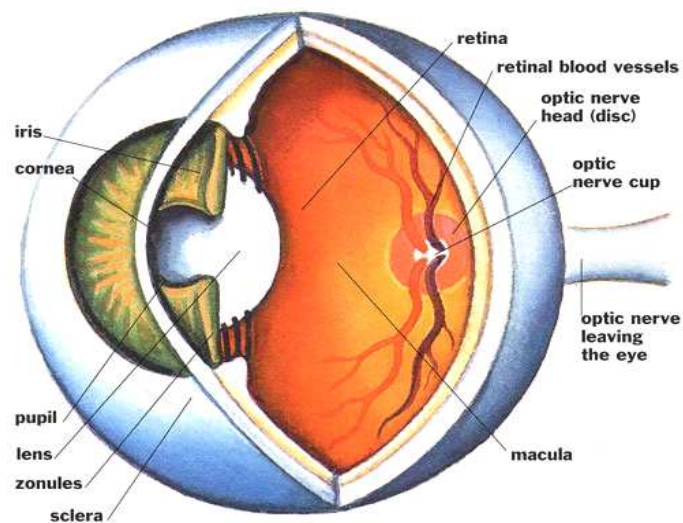


Fig.1 Sectional View of the Human Eye [26]

1.1 Literature Review

The heat transfer phenomena in human eye has been of major interest for the past century with various kinds of techniques being utilized to measure temperature profile within the eye. Invasive techniques used in earlier days in measuring the eye temperature are now confined to animal experiments due to its damaging nature of test procedures [16].

In the early 1950s, non-invasive techniques using a bolometer were used to obtain temperature reading of a cornea surface [10]. Infrared (IR) imaging technique has been widely used in measuring the temperature of the eye ever since. Efron et al. [3] reported results of the ocular surface temperature (OST) using IR imaging approach to have a mean of 34.3 °C while the paper by Purslow et al. [17] reported a mean of 35.0±1.1 °C. The difference is probably caused by various factors affecting the OST such as environmental conditions [18, 11], blinking [3, 11] and age [12]. Fielder et al. [4] using the same IR imaging technique reported that the center of the cornea is 3.6 °C lower than the body temperature.

In 1975, Taflove and Brodwin [22] applied the finite difference method (FDM) to model heat transfer across the human eye. A peak temperature of 39.3 and 40.4 °C was obtained for the 750 and 1500 MHz radiation, respectively, for an incident heat flux of 1000 W/m². In their model the properties in the eye are assumed to be homogeneous and similar to water. Subsequent study by Legendijk [9] showed that the thermal conductivity of the lens is much lower than that of water. The model however neglected other components inside the eye such as cornea and the iris which can cause significant error. Guy et al. [6] used the finite element method (FEM) to investigate the effects of 2450 MHz radiation on rabbit eyes. The model incorporated boundary conditions which included evaporation and radiation from the cornea surface. The eye was assumed to have homogeneous properties. The assumption that lens thermal conductivity is 0.213 W/m K did not match with experimental values [9]. A peak temperature of 40.0 °C for an incident irradiation of 1000 W/m² was found to be located at the back of the lens. Legendijk [9] conducted measurements on rabbits' eyes and used the results to predict thermal properties of the rabbit eye using FDM. The measured temperature was 34.5 ± 0.7 °C at the cornea surface whereas the calculated temperature using the FDM model presented a temperature of 34.20 °C at the same location. The FEM model by Scott [20] was a 2D model symmetrical at the pupillary axis. It consisted of six regions with boundary conditions employed on the surface of the cornea and the sclera. The cornea surface temperature predicted was 33.25 °C which deviates from measured temperatures using invasive and non-invasive techniques [16, 10].

Recently, Chua et al. [2] have numerically predicted the temperature distribution within the human eye when subjected to a laser source using the Finite Volume method (FVM) based on rectangular parallelepiped geometry of the eye. They used Pennes bioheat transfer equation [15]. Their results show good agreement between the model and experimental data up to 5%. Ng and Ooi [13] presented a 2D steady state FEM model of human eye using bioheat analysis. The results were satisfactorily validated with experiments and computations done by earlier researchers on human as well as animal eyes. In a subsequent work Ng and Ooi [14] developed a 3D FEM model of the human eye to obtain steady state temperature

distribution during normal condition and during electromagnetic (EM) wave radiation. The actual geometry of the eye, that is, close to a sphere was used. Results show a discrepancy of 0.49% for a normal condition as opposed to 1.9% of a 2D model when compared with experimental results from open literature. Their results for EM radiation are in reasonable agreement with the simulated results computed by an earlier report.

1.2 Objectives of the Present Work

The literature review indicates that while FDM, FVM and FEM techniques have been used, and rectangular parallelepiped and spherical geometries have been assumed for the eye, so far no attempt has been made to model the human eye as a cylinder. The main objective of this work is to develop an FDM based computational heat transfer model for laser eye surgery using two kinds of geometry of the eye, namely, rectangular parallelepiped and cylindrical. The idea is to see which geometry gives better prediction with respect to experimental measurements. In addition to the above, other aim of this study is to conduct a parametric study in order to understand the effect of laser power-off periods on its temperature distribution. The literature review also reveals that so far only insulation boundary condition on the periphery of eye has been used by earlier researchers. While the results in the first part of this paper are based on insulation boundary condition on the eye periphery another objective is to see the effects of other types of boundary condition such as convection and constant temperature (37°C) on the temperature distribution in the eye.

Nomenclature

C	Specific heat of eye tissues (kJ / kg K)
c_b	Specific heat of blood (kJ / kg K)
D	Characteristic length (m)
g	Acceleration due to gravity (9.8 m/s ²)
h_b	Heat Transfer Coefficient from the eye periphery to the surrounding tissue (W/m ² K)
h_c	Convective heat transfer coefficient from cornea to air (W/m ² K)
k	Thermal Conductivity of Eye tissues (W/m K)
Pr	Prandtl number of air
q''	Heat flux on the eye surface due to laser source (W/m ²)
q_e''	Heat flux due to evaporation (W/m ²)
q'''	Heat generation with the eye tissues per unit volume due to laser heat absorption (W/m ³)
r	radial coordinate(m)
T	Temperature of Eye (K)

T_{amb}	Atmospheric Temperature (K)
T_b	Blood Temperature (K)
t	time(s)
x,y,z	Cartesian coordinates(m)

Greek Symbols

β	Volumetric coefficient of thermal expansion of air (K ⁻¹)
ε	Emissivity at the cornea surface
λ	Absorption coefficient (m ⁻¹)
ρ	Density of Eye tissues (Kg / m ³)
σ	Stefan-Boltzmann constant (5.67 x 10 ⁻⁸ W/m ² K ⁴)
ν	Kinematic viscosity of air (m ² / s)
ω	Blood perfusion rate (m ³ of blood / m ³ of tissue per second)

Subscripts

a	Air
b	Blood
c	Convection
s	Surface

2.0 Problem Formulation

2.1 Assumptions

The assumptions made in the modeling are as follows.

- (1) The human eye is a semi-transparent solid structure and a composite consisting of the various tissues in contact with each other.
- (2) The tissue thermophysical properties for each region are homogenous and isotropic.
- (3) The heat that is impinging on the surface of the eye is absorbed in the eye at a decreasing rate with highest absorption being near the surface.
- (4) The eye's cooling mechanism is located at the surface of the eyeball (cornea).
- (5) The eye is symmetrical about the pupillary axis.
- (6) The absorption probability of ocular tissue is modulated based on the Lambert-Beer's law to reproduce the exponential attenuation of the laser light with depth within a biomaterial.
- (7) The effect of free convection currents in the aqueous humour region of the eye due to laser heating has been neglected. This can only be considered in non-Pennes bio heat transfer equation which considers the fact that there is no vascularization in aqueous region or for that matter in vitreous and cornea.
- (8) The laser input energy is considered as uniform across the cornea surface.

2.2 Rectangular Parallelepiped Geometry

The physical domain is shown in Fig.2. The relevant dimensions [1, 2, 13] are indicated in the figure.

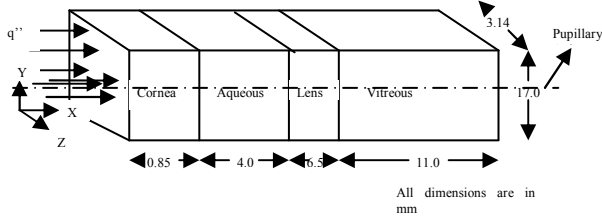


Fig.2 Rectangular Parallelepiped Geometry of the Human Eye (Physical Domain)

2.2.1 Governing Equation

The classic Pennes [15] bioheat transfer equation (eq.(2.1)) which is derived for an idealized tissue system with blood vessels through it describes the heat transfer within a tissue. In this equation, the metabolic heat generation term is neglected as it is generally much smaller than the external heat deposited [8].

$$\rho C \frac{\partial T}{\partial t} = \frac{\partial}{\partial x} \left(k \frac{\partial T}{\partial x} \right) + \frac{\partial}{\partial y} \left(k \frac{\partial T}{\partial y} \right) + \frac{\partial}{\partial z} \left(k \frac{\partial T}{\partial z} \right) + \omega_b C_b \rho_b (T_b - T) + q''' \quad (2.1)$$

Equation (2.1) is valid in each region of the eye tissue.

2.2.2 Initial and Boundary Conditions

Except for the validation the initial temperature is taken as 37°C, same as body temperature.

The computational domain is one fourth of the cross-section of the eye considering the thermal and geometrical symmetry of the problem about the pupillary axis. Heat lost from the corneal surface exposed to the surrounding air was mainly by convection. Over the remaining part of the eyeball, cooling was achieved by means of the high blood flow in the capillaries that run through the interior of the eyeball.

The boundary condition for temperature at the surface of the eye in the cornea region exposed to the air was written as

At $x = 0$,

$$-k_s \frac{\partial T}{\partial x} = h_c (T_{amb} - T_s) + \sigma \epsilon (T_{amb}^4 - T_s^4) + q_e'' \quad (2.2)$$

q_e'' is the heat loss per unit area due to evaporation of tears from the cornea surface and its value is taken as 20 W/m²[13].

The convective heat transfer coefficient under free convection was calculated for a flat square plate using the following relationship [2]. T_{amb} is taken as 298 K.

$$h_c = 0.54 k_a \left[\frac{g \beta (T_s - T_{amb}) \text{Pr}}{D \nu^2} \right]^{0.25} \quad (2.3)$$

where D is taken as the vertical dimension of the cross-section of the eye.

At the interfaces the compatibility conditions, that is, equality of temperature and continuity of heat flux have to be satisfied.

In addition, the end surface and the non-axial side surfaces are considered to be insulated.

2.3 Cylindrical Geometry

The physical domain is shown in Fig.3. The relevant dimensions [1, 2, 13] are indicated in the figure. It may be noted that the diameter of the cylinder is taken as equal to the height of the rectangular parallelepiped.

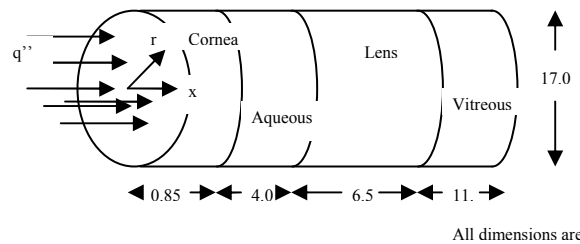


Fig 3: Cylindrical Geometry of the Human Eye (Physical Domain)

2.3.1 Governing Equation

The classic Pennes bioheat transfer equation that describes the heat transfer within a tissue is given in cylindrical coordinates for axi-symmetric surface boundary condition (eq.(2.4)).

$$\rho C \frac{\partial T}{\partial t} = k \left(\frac{\partial^2 T}{\partial r^2} + \frac{1}{r} \frac{\partial T}{\partial r} + \frac{\partial^2 T}{\partial x^2} \right) + \omega_b C_b \rho_b (T_b - T) + q''' \quad (2.4)$$

Equation (2.4) is valid in each region of the eye.

2.3 Initial and boundary conditions

Except for the validation the initial temperature is taken as 37°C, same as body temperature. Because of axial symmetry, $T = T(r, x)$.

The boundary condition for temperature at the surface of the eye in the cornea region exposed to the air is written as:

At $x = 0$,

$$-k_s \frac{\partial T}{\partial r} = h_c (T_{amb} - T_s) + \sigma \varepsilon (T_{amb}^4 - T_s^4) + q_e'' \quad (2.5)$$

Where h_c can be calculated as [2] :

$$h_c = 0.54 k_a \left[\frac{g \beta (T_s - T_{amb}) \text{Pr}}{(D V)^2} \right]^{0.25} \quad (2.6)$$

D is taken as the diameter of the cylinder.

Due to axi-symmetry:

$$\text{At } r = 0, \quad \frac{\partial T}{\partial r} = 0 \quad (2.7)$$

At the tissue interfaces the compatibility conditions have to be satisfied.

In addition, the end surface and the peripheral surface of the eye are considered to be insulated.

2.4 Absorption of Laser Light within the Tissue

The absorption property of ocular tissue has been taken into account to model external energy deposition because of laser used in eye surgery. This absorption property is based on the Lambert-Beer's law and it considers exponential attenuation of the laser light with depth within a biomaterial [25]. The heat flux can be written as:

$$q'' = q_o'' e^{-\lambda x} \quad (2.8)$$

where the absorption coefficient $\lambda = 8 \text{ m}^{-1}$. q_o'' is the heat flux impinging on the left surface of each region of the eye tissue and its value at the cornea surface is the laser power which is known.

$$q_i''' = \frac{q'' A}{V_i} \quad (2.9)$$

where A is the cross-sectional area and V_i is the volume of the tissue in the i th region, where $i = 1$ (cornea), $i = 2$ (aqueous), $i = 3$ (lens) and $i = 4$ (vitreous).

3.0 Method of Solution

An explicit finite-difference scheme has been used. The reason for the use of FDM is the regular geometry of the computational domain. FVM and FEM are particularly useful for handling irregular geometries. The time-step has been chosen based on the stability criteria. In the discretized equations the coefficients of the temperature at the present time at the interior, boundary and corner grid points have to be positive for stable solution. Using the aforesaid criterion the allowable time-step required for stability is computed. A grid independence test has been performed for both the geometries. The number of grid points for the rectangular parallelepiped geometry is $30 \times 20 \times 5$ in x, y and z-direction, respectively, and time-step is 0.198 s. The number of grid points for the cylindrical geometry is 60×40 in x and r-direction, respectively and the time-step is 0.059 s.

4.0 Results and Discussion

4.1 Thermophysical Properties

The results are presented based on the thermophysical properties of the ocular tissues and blood as given in Table 1. The blood perfusion rate (ω_b) is $4.5 \times 10^{-3} \text{ s}^{-1}$. The source of the property values is Waddell et al. [23] and Ng and Ooi[13]. The emissivity of the cornea surface (ε in eqs.(2.2) and (2.5)) is taken as 0.975[13].

Table 1 Thermophysical Properties of the Ocular Tissues and Blood

	k (W/m K)	C (J/kg K)	ρ (kg/m ³)
Cornea	0.58	4178	1057
Aqueous	0.58	3997	996
Lens	0.4	3000	1050
Vitreous	0.603	4178	1000
Blood	-	3780	1060

4.2 Validation of the Present Numerical Results

The results show no variation of temperature in the cross-section of the eye. Thus, temperature distribution is essentially one-dimensional. This is not surprising as on the periphery insulation boundary conditions have been imposed. The present model has been validated by comparing predictions from the model with experimental results obtained by Waddell et al. [23] under in vitro clinical setting as well as with the numerical results of Chua et al. [2] when $q'' = 0$ and initial temperature is 25°C. Here, in this case blood which is entering the arteries at 37°C is heating the surrounding tissue. Comparisons are made for temperature at the centre of each ocular tissue along the central axis of the human eye. Fig.4 depicts the predictions based on rectangular parallelepiped and cylindrical geometries and the corresponding results from experiment [23] and another numerical model [2]. It is clear from the T vs. t plot that the model rectangular parallelepiped

geometry gives results close to experiment. The reason why cylindrical geometry based model predicts higher temperature is due to higher volume of the cylinder and hence larger heat generation. The rectangular parallelepiped geometry reaches equilibrium faster because it has lower volume to surface area ratio than that of cylindrical geometry and experimental model. However, FVM model of Chua et al.[2] with which the present results are compared does not mention the length of tissue in each region of the eye and therefore, it is difficult to say why steady state reached later for the FVM model.

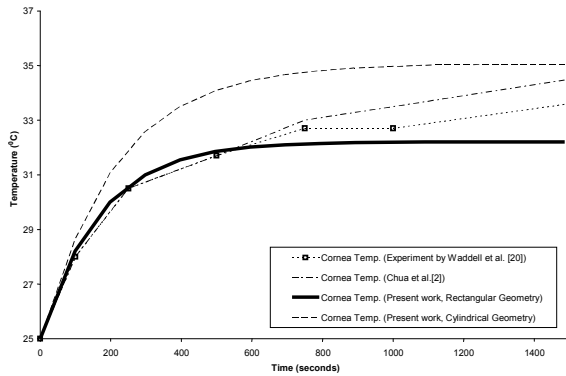


Fig.4 Validation of the Present Results showing cornea temperature for $q'' = 0 \text{ W/m}^2$ and initial temperature 25°C

4.3 Results for Rectangular Geometry

4.3.1 Ocular Tissue Interface Temperature vs. Time

Figure 5 shows the eye tissue interface temperature vs. time for rectangular geometry when $q'' = 2000 \text{ W/m}^2$ and initial temperature is 37°C . The plots indicate cornea-aqueous interface is at the highest temperature as expected and the steady state is reached at 800 s (13.3 minutes). The rate of change of temperature with respect to time is greatest for cornea-aqueous interface. The results also indicate that at high power density it is essential to wear protective eye-wear to prevent extreme thermal damage due to industrial accidents.

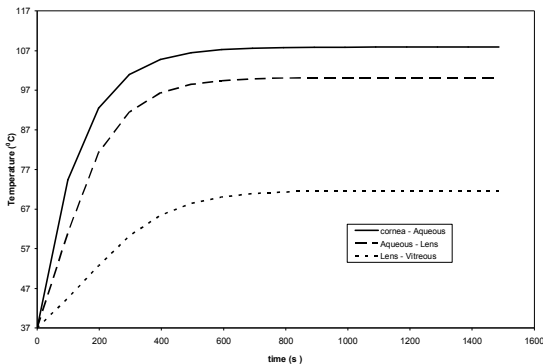


Fig. 5 Temperature at interfaces of ocular tissues vs Time for $q'' = 2000 \text{ W/m}^2$

4.3.2 Temperature along the Axis of Eye at Various Times

Figure 6 shows axial temperature distribution in the eye at various times. The results indicate that at the steady state the temperature varies from 108°C at the cornea surface to 55°C at the end of vitreous. The large axial temperature gradient also implies that lumped system analysis would give erroneous results. The small axial temperature gradient in the cornea as revealed in Fig.6 justifies the use of small number of grid points in the axial direction in the cornea region.

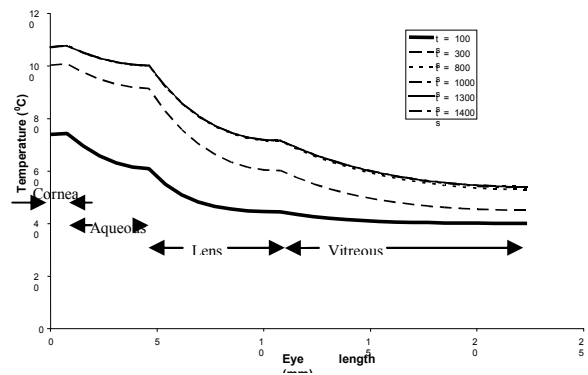


Fig.6 Temperature along the axial distance in the eye at various times for $q'' = 2000 \text{ W/m}^2$

4.3.3 Effect of Time-Varying Laser Fluence

In laser surgery sometimes surgeons conduct the operation in stages with short intervals of 1 or 2 min. The present model simulated a surgical process with a two 1-min laser-off periods for an 11-min ocular surgery. Figures 7-10 depict the transient temperatures in various regions of the eye during intermittent laser surgery. The results reveal that cornea experiences the largest temperature drop followed by aqueous, lens and vitreous. It is mainly due to higher temperature gradient between cornea and the surrounding air.

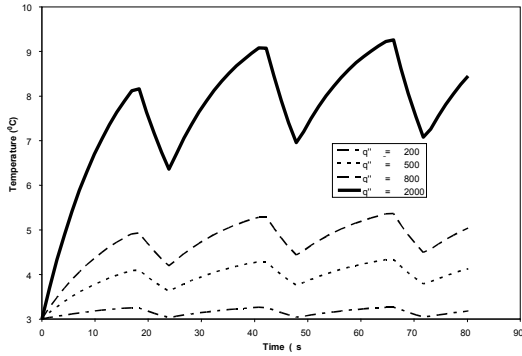


Fig 7: Cornea Temperature vs time for intermittent laser

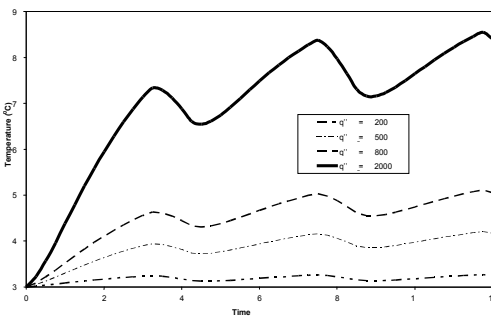


Fig 8: Aqueous Temperature vs time for intermittent laser

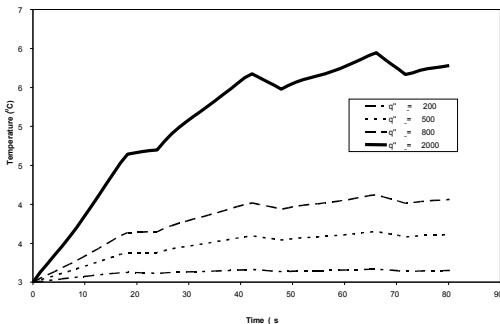


Fig 9: Lens Temperature vs time for intermittent laser

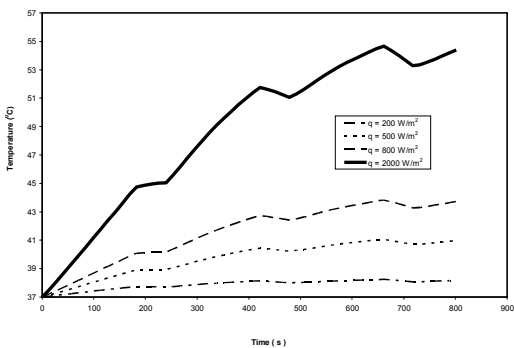


Fig 10: Vitreous Temperature vs for intermittent laser

4.4 Comparison of Results for Rectangular and Cylindrical Geometry for $q'' = 2000 \text{ W/m}^2$ and initial temperature of 37°C

Figure 11 depicts temperature vs. time plots for cornea, aqueous, lens and vitreous for rectangular parallelepiped and cylindrical geometries of the eye for $q'' = 2000 \text{ W/m}^2$ and initial temperature of 37°C . It is interesting to note that for higher power of laser source and higher initial temperature the temperature predicted by cylinder-model is lower than that by rectangular parallelepiped model. This trend is opposite for much lower heat flux and lower initial temperature as shown in Fig.3. The reason may be due to larger heat loss due to larger exposed surface area of the cylinder and also greater temperature difference between cornea surface and the surrounding air at high heat flux.

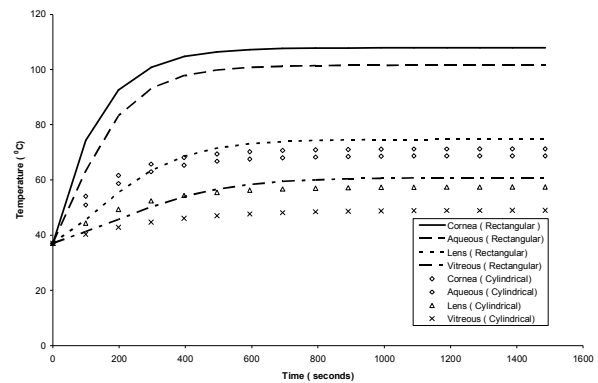


Fig. 11 Comparison of T vs. t plots in various regions of the eye for cylindrical and rectangular parallelepiped geometries for $q'' = 2000 \text{ W/m}^2$ and initial temperature of 37°C

4.5 Effect of Other Peripheral Boundary Conditions

In the foregoing sections of this paper the results based on the insulated periphery of the eye have been reported. The effects of two other peripheral boundary conditions on the temperature distribution within the eye have also been investigated. They are (i) Convection with $h_b = 10 \text{ W/m}^2\text{K}$ to blood at 37°C and (ii) constant temperature of 37°C .

4.5.1 Effect of Convective Peripheral Boundary

4.5.1.1 Rectangular Geometry

Figure 12 depicts isotherms at the cornea surface for laser heat flux of 200 W/m^2 at steady state. It may be noted that the computational domain shown is the lower right hand quarter of the cross-section of the physical domain because of symmetry. It is evident from the figure the heat transfer across the cross-section is two-dimensional. The changing pattern of isotherms

periphery model is close to that for other two boundary conditions at large time. However, for $q'' = 200 \text{ W/m}^2$ and initial temperature of 37°C (Fig.17) the model based on isothermal periphery predicts lowest temperature at the centre of the lens axis in comparison with other two models as $h_b \rightarrow \infty$.

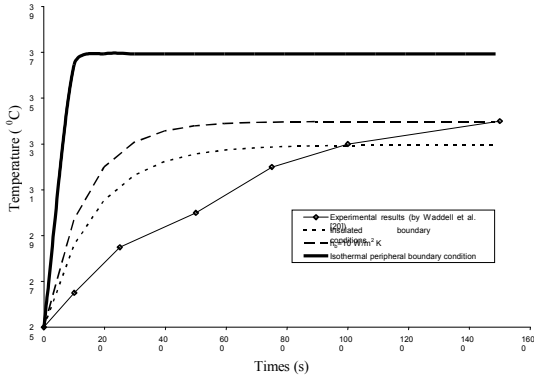


Fig.14: Comparison of Aqueous temperature for different peripheral boundary conditions for rectangular parallelepiped model and experimental results for initial temperature of 25°C and no heat flux ($q'' = 0$)

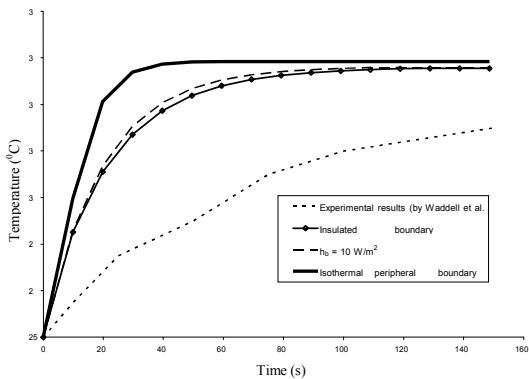


Fig.15: Comparison of Aqueous temperature for different peripheral boundary conditions for cylindrical model and experimental results for initial temperature of 25°C and no laser heat flux ($q'' = 0$)

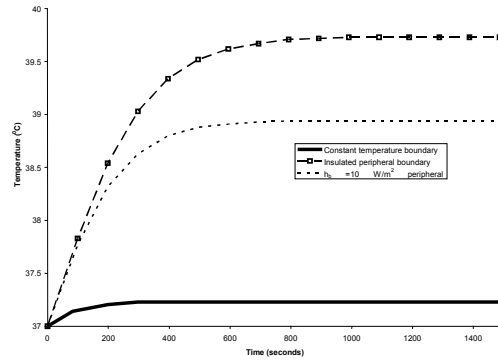


Fig.16 Comparison of Lens temperature for different peripheral boundary conditions for rectangular parallelepiped model for initial temperature of 37°C and $q'' = 200 \text{ W/m}^2$

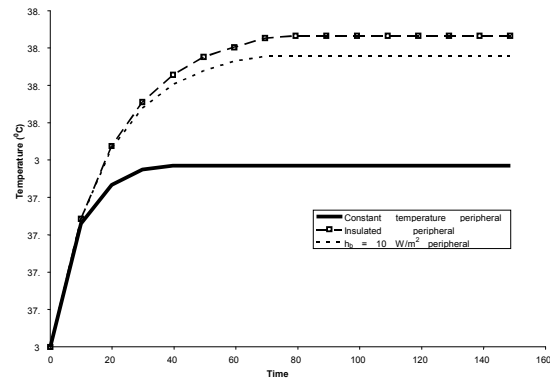


Fig.17 Comparison of Lens temperature for different peripheral boundary conditions for cylindrical model for initial temperature of 37°C and $q'' = 200 \text{ W/m}^2$

5.0 Conclusions

The present work simulates a laser eye surgery by a computational heat transfer model using Pennes bioheat transfer equation. Two geometries have been considered, namely, rectangular parallelepiped and cylindrical. The former predicts temperature of the eye close to in-vitro experiment for no laser heating ($q'' = 0 \text{ W/m}^2$) and initial temperature of 25°C for insulated periphery. Interestingly, the model based on cylindrical geometry predicts higher temperature for the aforesaid conditions. The opposite is true for high laser heating ($q'' = 2000 \text{ W/m}^2$) and initial temperature of 37°C . For intermittent laser sources, it is found that higher the initial power rating, the higher the reduction of temperature within the ocular tissues when the laser was shut off. The cornea experiences the greatest fall of temperature followed by aqueous chamber, lens and vitreous, respectively. A comparison of the results based on three different peripheral boundary conditions such as convection, constant temperature

and insulation reveals that the model based on insulation condition on the eye periphery predicts temperature closest to experiment when $q'' = 0$ and initial temperature is 25°C. However, when the laser power is 200 W/m² and the initial temperature is 37°C the insulation condition imposed on the eye periphery produces highest temperature followed by that produced by convection and constant temperature conditions. The heat transfer is one-dimensional, that is, only in the axial direction from the cornea to vitreous when the eye periphery is insulated whereas for the conditions of convection and constant temperature the heat transfer is multi-dimensional, that is, three-dimensional in case of rectangular parallelepiped and two-dimensional in case of cylindrical geometry. The dimensional effects become stronger when the magnitude of the laser heat flux on cornea increases.

Further effort may be directed towards modeling the eye as a sphere. During a laser surgery, free convection currents in Aqueous humour can be significant. This can only be incorporated into a non-Pennes bio heat transfer model.

References

1. Charles M. W., Brown Nicholas, 1975, "Dimensions of the Human Eye Relevant to Radiation Protection", *Physics Med. Biol.*, Vol. 20, No. 2, pp. 202-218.
2. Chua K.J., Ho J.C., Chou, S.K., Islam, M.R., 2005, "On the study of temperature distribution within a human eye subjected to a laser source", *International Communications in Heat and Mass Transfer*, Vol. 32, pp. 1057-1065.
3. Efron N., Young G., Brennan, 1989, "Ocular Surface Temperature", *Current Eye Research*, Vol. 8, pp. 901-906.
4. Fielder A.R., Winder A.F., Sheridaiah G.A.K. et al., 1981, "Problems with corneal arcus", *Trans. Ophthalmol. Soc. UK*, Vol. 101, pp. 22-26.
5. Gros, C., Bronner A., Vrousos C., 1967, *J. Radiol. Electrol.*, Vol. 48, 95
6. Guy A., Lin J.C., Kramar P.O., Emery A.F., 1975, "Effect of 2450-MHz radiation on the rabbit eye", *IEEE Trans. Microw. Theory Tech. MTT-23*, Vol.6, pp. 492-498.
7. Huber A. 1960, *Ophthalmologica (Basel)*, Vol.139, p.351
8. Jain R. K., 1983, *Hyperthermia in Cancer Therapy*, Hall Publication, Boston.
9. Lagendijk J.J.W., 1982, "A Mathematical model to calculate temperature distributions in human and rabbit eyes during hyperthermic treatment", *Phys. Med. Biol.*, Vol. 27 (11), pp. 1301-1311.
10. Mapstone R., 1968, "Measurement of corneal temperature", *Experimental Eye Research*, Vol. 7, pp. 237-243.
11. Mapstone R., 1968, "Determinants of ocular temperature", *Br. J. Ophthalmol.*, Vol. 52, pp. 729-741
12. Morgan P.B., Soh M.P., Efron N., 1999, "Corneal surface temperature decrease with age", *Contact Lens Anterior Eye*, Vol. 22 (1), pp. 11-13.
13. Ng. E.Y. K., Ooi E. H., 2006, "FEM simulation of the eye structure with bioheat analysis", *Computer methods and programs in biomedicine*, Vol. 82, pp. 268-276.
14. Ng. E.Y. K., Ooi E. H., 2007, "Ocular surface temperature: A 3D FEM prediction using bioheat equation", *Computers in Biology and Medicine*, Vol. 37, pp. 829 - 835.
15. Pennes H.H., 1948, "Analysis of tissue and arterial blood temperatures in the resting human forearm", *Journal of Applied Physiology*, Vol.1, pp. 93-122
16. Purslow C., Wolffsohn J., 2005, "Ocular surface temperature, a review", *Eye contact Lens*, Vol. 31, pp. 117-123.
17. Purslow C., Wolffsohn J., Santodomingo-Rubido J., 2005, "The effect of contact lens wear on dynamic ocular surface temperature", *Contact Lens Anterior Eye*, Vol. 28, pp. 29-36.
18. Schwartz B., 1965, "Environmental temperature and the ocular temperature gradient", *Arch. Ophthalmol.* Vol.74, pp. 237-243.
19. Scott J.A., 1988, "The computation of temperature rises in the human eye induced by infrared radiation", *Physics Med. Biol.*, Vol. 33, No 2, pp.243-257.
20. Scott J.A., 1988, "A finite element model of heat transport in the human eye", *Phys. Med. Biol.*, Vol. 33 (2), pp. 227-241
21. Sekins K.M., Emery A.F., in: J.F. Lehmann (Ed.), 1982, *Therapeutic Heat and Cold*, Williams and Wilkins Publisher, Baltimore.
22. Taflove A., Brodwin M., 1975, "Computation of the electromagnetic fields and induced temperatures within a model of the microwave-irradiated human eye", *IEEE Trans. Microw. Theory Tech. MTT-23* (11), pp. 888-896.
23. Waddell D. E., Rylander H.G., Ghaffari, Diller K.R., Farrar R.M., in: J.J. McGrath (Ed.), 1992, *Advances in Biological Heat and Mass Transfer*, ASME HTD, Newyork.
24. Zeiss E. 1930, *Arch. Augenheilk.*, Vol.102, p.523.
25. Zhigilei L.V., Garrison B.J., 2000, "Microscopic mechanism of laser ablation of organic solids in the thermal and stress confinement irradiation regimes", *Journal of Applied Physics*, Vol. 88, No. 3, pp. 1281-1298.
26. <http://www.lighthouse.org/images/eye.jpg>